

Squeeze-out of nuclear matter in peripheral heavy-ion collisions and momentum-dependent effective interactions. *

A. B. Larionov [†], W. Cassing, C. Greiner, U. Mosel

Institut für Theoretische Physik, Universität Giessen, D-35392 Giessen, Germany

Abstract

We perform a systematic study of in-plane and out-of-plane proton and neutron flow from nucleus-nucleus collisions within the BUU transport approach employing different parameter sets for the mean-field potentials that can be characterized by the nuclear incompressibility and the stiffness of the momentum-dependent potential. We find that a simultaneous description of the experimental data from the BEVALAC and the SIS on both the nucleon squeeze-out v_2 and the in-plane flow F at beam energies $E_{lab} = 0.15 \div 2$ AGeV requires a mean field with strong momentum dependence, i.e. an effective Landau mass $m^* \simeq 0.68m_0$ at normal nuclear matter density $\rho_0 = 0.17$ fm⁻³, where $m_0 = 0.938$ GeV is the bare nucleon mass. Some experimental data on the squeeze-out require an even stiffer momentum dependence ($m^* \approx 0.62 m_0$). All systems investigated are found to be compatible with $m^*/m_0 = 0.65 \pm 0.03$.

PACS numbers: 25.70.-z; 25.75.-q; 25.75.Ld; 21.65.+f

Keywords: Heavy-ion collisions; Collective flow; Transport models; Equation of state; Effective mass

*Supported by BMBF and GSI Darmstadt

[†]On leave from RRC "I.V. Kurchatov Institute", 123182 Moscow, Russia

I. INTRODUCTION

Since many years the study of the various collective flows of nuclear matter is one of the main subjects in heavy-ion physics [1–9]. The interest in collective nuclear motion under extreme conditions, like high density and/or high temperature, originates from the fundamental problem to extract the equation of state (EOS) of nuclear matter. It was shown in Refs. [10–13] that the in-plane directed flow [14] is sensitive to both the incompressibility K of the EOS and to the momentum-dependent effective interaction (MDI). Moreover, the in-medium nucleon-nucleon (NN) cross section (that is related to the imaginary part of the in-medium G -matrix) also influences the transverse directed flow [15] since nucleons acquire transverse momentum also by elastic and inelastic collisions. It is necessary, therefore, to have at least two additional observables, besides the in-plane flow, in order to determine the three most commonly used components of the effective NN interaction adopted in the various analyses: the incompressibility K , the stiffness of the MDI and, possibly, the in-medium NN cross section.

The rapidity distribution of nucleons, which is only weakly dependent on the mean-field parameters, gives reasonable constraints on the in-medium NN cross section or on the nuclear stopping power [16,17]. However, it was not so clear until recently, how to possibly extract information on the MDI from heavy-ion collisions. Danielewicz [18] has shown within the Boltzmann-Uehling-Uhlenbeck (BUU) transport model, that the elliptic flow (or squeeze-out ratio) of protons at midrapidity is very sensitive to the MDI part of the nucleon mean field. The reaction Bi+Bi at $E_{lab}=400, 700, 1000$ AMeV (measured by the KAOS Collaboration [19]) has been analysed in [18] leading to the conclusion that the MDI part of the NN interaction should produce an effective Landau mass $m^* \simeq 0.7m_0$, since momentum independent forces ($m^* = m_0$) strongly underpredict the squeeze-out ratio at high transverse momenta [18].

The aim of our present work is: (i) to study the mechanism of the squeeze-out enhancement by the MDI and (ii) to analyse several independent data sets on the *directed* and *elliptic*

flow of nucleons to get experimental constraints on the stiffness of the MDI. We concentrate on the bombarding energy regime up to 2 AGeV since here multiple meson production or "string" degrees of freedom play a minor role. As shown by Sahu et al. [20] the collective flow is strongly influenced by the effective degrees of freedom taken into account in the transport approach at high energies. For a detailed investigation of this problem – especially at AGS energies – we refer the reader to Ref. [20].

The paper is structured as follows: In Sect. II a brief description of the applied BUU model is given. Sect. III contains our interpretation of the squeeze-out mechanism which is illustrated in Sect. IV by a detailed study of the time evolution of colliding nuclear systems within BUU calculations. A comparison to the experimental data on the proton and neutron elliptic and directed flows is given in Sect. V, while Sect. VI concludes our work with a summary of the results.

II. THE BUU MODEL

In our calculations we have applied the recent version of the BUU model described in more detail in Ref. [21]. The equation of motion for the nucleon phase-space distribution function $f(\mathbf{r}, \mathbf{p}, t)$ includes a propagation in the momentum-dependent scalar mean field $s(\mathbf{r}, \mathbf{p}, f)$ via the single-particle energy

$$H_{mf}(\mathbf{r}, \mathbf{p}, t) = \sqrt{(m_0 + s(\mathbf{r}, \mathbf{p}, f))^2 + p^2} . \quad (1)$$

Both elastic and inelastic scattering processes are additionally described by the r.h.s. of the transport equation

$$\begin{aligned} & \left(\frac{\partial}{\partial t} + \frac{\partial H_{mf}}{\partial \mathbf{p}_1} \frac{\partial}{\partial \mathbf{r}} - \frac{\partial(H_{mf} + U_{Coul})}{\partial \mathbf{r}} \frac{\partial}{\partial \mathbf{p}_1} \right) f(\mathbf{r}, \mathbf{p}_1, t) \\ & = g \int \frac{d\mathbf{p}_2}{(2\pi\hbar)^3} \int d\Omega v_{12} \frac{d\sigma_{NN}(p_{12})}{d\Omega} (f_3 f_4 (1 - f_1)(1 - f_2) - f_1 f_2 (1 - f_3)(1 - f_4)) \\ & + \text{coupling terms} , \end{aligned} \quad (2)$$

where U_{Coul} is the Coulomb potential acting on protons; $g = 4$ is the spin-isospin degeneracy of a nucleon; $v_{12} = |\mathbf{v}_1 - \mathbf{v}_2|$ and $p_{12} = |\mathbf{p}_1 - \mathbf{p}_2|$ are the relative velocity and relative momen-

tum of colliding nucleons, respectively; $d\sigma_{NN}(p_{12})/d\Omega$ is the energy dependent differential NN scattering cross section as parametrized by Cugnon [22]; $f_i := f(\mathbf{r}, \mathbf{p}_i, t)$ ($i = 1, 2, 3, 4$), while \mathbf{p}_3 and \mathbf{p}_4 are the final momenta of the scattered nucleons. The coupling terms in (2) account for the various inelastic channels: $NN \Leftrightarrow \pi NN$, $NN \Leftrightarrow NR$ – S-wave pion and resonance production/absorption, $NN \rightarrow \Lambda KN$, $NN \rightarrow \Sigma^0 KN$ – strangeness production.

The scalar potential $s(\mathbf{r}, \mathbf{p}, f)$ is computed as follows (see [23]):

1) In the local rest frame (l.r.f.) of the nuclear matter element, where the space components of the baryonic 4-current $j^\mu = (j^0, \mathbf{j})$ vanish, i.e. $\mathbf{j} = 0$, the single-particle energy is calculated as

$$\epsilon_{l.r.f.}(\mathbf{r}, \mathbf{p}) = \sqrt{m_0^2 + p^2} + U(\rho, \mathbf{p}) . \quad (3)$$

The explicit form of the momentum-dependent potential U in (3) is taken from Welke et al. [24] as

$$U(\rho, \mathbf{p}) = A \frac{\rho}{\rho_0} + B \left(\frac{\rho}{\rho_0} \right)^\tau + \frac{2C}{\rho_0} \int \frac{gd\mathbf{p}'}{(2\pi\hbar)^3} \frac{f(\mathbf{r}, \mathbf{p}')}{1 + (\mathbf{p} - \mathbf{p}')^2/\Lambda^2} . \quad (4)$$

A symmetry energy term is not taken into account in the potential (4).

2) The mean field s is calculated from the relation in the l.r.f.

$$s = \sqrt{\epsilon_{l.r.f.}^2 - p^2} - m_0 . \quad (5)$$

3) The scalar potential s is then used in Eq. (1) to determine the single-particle energy in the computational frame. Steps 1)-3) are repeated until selfconsistency is reached, i.e. s is not changed within the accuracy of numerics on the level of 10^{-4} .

The interaction range Λ of the potential (4) is chosen as in Ref. [24]: $\Lambda = 1.5p_F^{(0)}$, where $p_F^{(0)} \equiv p_F(\rho_0)$, $p_F(\rho) = (\frac{3}{2}\pi^2\rho)^{1/3}\hbar$. The residual four free parameters A , B , τ and C of the potential U are determined from the conditions:

(i) The effective mass at the Fermi surface

$$(m^*)^{-1} = m_0^{-1} + (p_F^{(0)})^{-1} \frac{\partial U}{\partial p} \Big|_{p=p_F^{(0)}} \quad (6)$$

must be in the range $0.6m_0 \leq m^* \leq m_0$ (c.f. [25,26]). This condition puts limits on the stiffness C of the MDI.

(ii) The energy per nucleon in nuclear matter has a minimum at $\rho = \rho_0$ and

(iii) a value of -16 MeV at the minimum:

$$\left. \frac{\partial \epsilon / \rho}{\partial \rho} \right|_{\rho=\rho_0} = 0, \quad \left. \frac{\epsilon}{\rho} \right|_{\rho=\rho_0} = -16 \text{ MeV}, \quad (7)$$

where

$$\begin{aligned} \epsilon(\rho) = & \frac{3}{5} \epsilon_F \rho + \frac{1}{2} A \frac{\rho^2}{\rho_0} + \frac{1}{\tau + 1} B \frac{\rho^{\tau+1}}{\rho_0^\tau} + \\ & \frac{C}{\rho_0} \int \frac{g d\mathbf{p}_1}{(2\pi\hbar)^3} \frac{g d\mathbf{p}_2}{(2\pi\hbar)^3} \frac{f(\mathbf{p}_1) f(\mathbf{p}_2)}{1 + (\mathbf{p}_1 - \mathbf{p}_2)^2 / \Lambda^2} \end{aligned} \quad (8)$$

with $\epsilon_F = p_F^2 / 2m_0$ and $f(\mathbf{p}) = \Theta(p_F - p)$. Explicit forms of the momentum integrals in (6),(8) are given in Ref. [24].

(iv) The nuclear matter incompressibility

$$K = 9\rho_0^2 \left. \frac{\partial^2 \epsilon / \rho}{\partial \rho^2} \right|_{\rho=\rho_0} \quad (9)$$

is fitted in the range $K = 200 \div 380$ MeV.

We have applied in our calculations the following mean fields denoted by H (hard, without momentum dependence), HM and SM (hard and soft, with a "standard" momentum dependence) as well as the new mean-field parametrization which is dubbed HM1 (see below). The parameters of all interactions are presented in Table 1. The stiffness C of the MDI in the interactions HM and SM is close to that of Ref. [24]. The set of parameters HM1 includes an MDI stiffness that is about 30% larger than in HM and SM, which leads to a smaller effective mass at the Fermi momentum for HM1. In Fig. 1 we show the resulting energy per nucleon as a function of density and the potential $U(\rho, p)$ versus momentum for several densities. The interactions H, HM and HM1 give practically the same EOS ($E/A(\rho)$ -dependence), but they differ in the MDI part, i.e. in their momentum dependence. This gives the possibility to extract an independent information on the MDI stiffness C . On the other hand, the interactions HM and SM produce different EOS, but have the same MDI, which is relevant for a separate study on the sensitivity to the incompressibility K .

III. SQUEEZE-OUT MECHANISM

A squeeze-out of nucleons is observed experimentally in the beam energy range below $1 \div 2$ AGeV where mean-field effects still play an essential role. It can be interpreted, however, to a major extent in terms of a shadowing phenomenon [5], as in the participant-spectator picture of a heavy-ion collision the fireball particles – emitted in the reaction plane – are rescattered on the spectators. This results intuitively in a squeeze-out ratio $R_N := (N(90^\circ) + N(270^\circ))/(N(0^\circ) + N(180^\circ))$ at midrapidity being larger than 1. Here $N(\phi)$ is the azimuthal distribution of nucleons with respect to the reaction plane in a given rapidity interval. A specific particle emitted from the center-of-mass of a system and moving in transverse direction with velocity v_t will be shadowed by the spectator piece, if it reaches the spectator during the passage time $\Delta t = 2R/(v_p^{c.m.}\gamma)$ of the colliding nuclei. Here R is the radius of the nuclei (assumed to be equal for projectile and target), $v_p^{c.m.}$ is the projectile velocity in the center-of-mass system, and $\gamma = (\sqrt{1 - (v_p^{c.m.})^2})^{-1}$. A straightforward geometrical estimate then leads to the condition $v_t\Delta t/2 > R - b/2$, or

$$v_t > \frac{R - b/2}{R} \gamma v_p^{c.m.}, \quad (10)$$

where b is the impact parameter. One can see from (10) that at larger impact parameters b the lower limit of v_t becomes smaller, i.e. more particles will be shadowed and the squeeze-out ratio R_N will increase (c.f. later Fig. 12). This is simply related to a larger size ($\sim b$) of the spectator pieces in peripheral collisions. It is also evident, that for faster moving particles it is easier to fulfill the condition (10) and, therefore, the squeeze-out ratio should grow with the particle transverse velocity v_t (c.f. later Figs. 6,13).

The squeeze-out phenomenon can also be characterized by a negative elliptic flow v_2 (c.f. [27]) which appears in the Fourier expansion

$$N(\phi) \propto 1 + 2v_1 \cos(\phi) + 2v_2 \cos(2\phi) + \dots . \quad (11)$$

Neglecting thus higher order terms in (11), the following direct relation is obtained:

$$R_N \simeq \frac{1 - 2v_2}{1 + 2v_2}. \quad (12)$$

In (11) the elliptic flow v_2 is given as

$$v_2 = \left\langle \frac{p_x^2 - p_y^2}{p_x^2 + p_y^2} \right\rangle. \quad (13)$$

At higher beam energy (~ 10 AGeV), faster moving and Lorentz-contracted spectators do not shadow particles any more from the expanding fireball [20]. This results in $R_N \leq 1$ (or $v_2 \geq 0$) as observed in experiment [28].

The simple geometrical picture discussed above will be illustrated by the BUU phase-space evolution in the next section. Since the squeeze-out is related to the participant-spectator reaction mechanism (c.f. [29]), we expect a lower beam-energy limit of ~ 0.1 AGeV for $R_N > 1$. At even lower beam energies the mean-field effects lead to the formation of rotating nuclear systems [30] that emit particles predominantly in the reaction plane due to centrifugal forces, thus producing $R_N < 1$ (or $v_2 > 0$, c.f. later Fig. 7).

We have to note, however, that the shadowing scenario can not completely explain the squeeze-out phenomenon. For instance, a small but statistically significant increase of $-v_2$ at the beam energy ~ 0.4 AGeV (see later Fig. 7) with increasing incompressibility K can not be understood in the shadowing picture. This is, probably, a manifestation of a focussing of high momentum particles by the repulsive mean field as proposed in Ref. [18].

IV. BUU STUDY OF THE SQUEEZE-OUT TIME EVOLUTION

We study the system Au+Au at the beam energy $E_{lab} = 0.4$ AGeV and impact parameter $b = 6$ fm. Fig. 2 shows the time evolution of the central baryon density and of the NN collision rate for the HM and SM mean fields. In agreement with Fig. 1 (upper left panel), a slightly higher density and, as a consequence, a higher collision rate are reached in the case of the SM parametrization. However, the various EOS shown in Fig. 1 practically do not differ in the density interval $0 < \rho \leq 0.27$ fm $^{-3}$ probed in the collision. We do not expect,

therefore, to get clear constraints on the incompressibility K from our study of *peripheral* collisions and concentrate mainly on the MDI-part of the effective interactions.

As pointed out in Ref. [18] the p_t -dependence of the v_2 coefficient is very sensitive to the momentum dependence of the nuclear mean field. In order to understand this fact, we have performed calculations with the parametrizations H and HM of the mean field. Fig. 3 shows the average transverse velocity (a) and transverse momentum (b) of the midrapidity neutrons moving in- and out- of the reaction plane versus time. We observe that in the case of the HM parameter set $\langle v_t \rangle$ reaches a maximum at $t \simeq 17$ fm/c when also the central density and the collision rate are close to the maximum (Fig. 2). At this time the system shows the most compact configuration in space, i.e. the line connecting the centers of target and projectile spectators, is perpendicular to the beam (z -) direction (Fig. 4). However, in case of the H mean field the transverse velocity has no maximum (the peaks of $\langle v_t \rangle$ and $\langle p_t \rangle$ at $t \simeq 7$ fm/c are due to fluctuations, because initially there are no nucleons at midrapidity). Moreover, at $t < 40$ fm/c in the case of the HM mean field the average transverse velocity is larger than for the mean field H, while the transverse momentum is practically independent on the mean field, even showing a slightly opposite tendency: at $t < 40$ fm/c the mean field H produces a somewhat larger $\langle p_t \rangle$. This can be qualitatively understood from the Hamiltonian equations:

$$\dot{\mathbf{r}} = \frac{\partial H_{mf}}{\partial \mathbf{p}} = \frac{\mathbf{p}}{H_{mf}} + \frac{m_0 + s}{H_{mf}} \frac{\partial s}{\partial \mathbf{p}}, \quad (14)$$

$$\dot{\mathbf{p}} = -\frac{\partial H_{mf}}{\partial \mathbf{r}} = -\frac{m_0 + s}{H_{mf}} \frac{\partial s}{\partial \mathbf{r}}. \quad (15)$$

where H_{mf} is the single-particle energy (1). For the momentum-independent mean field H, (14) reduces to a simple proportionality: $\mathbf{v} = \mathbf{p}/H_{mf}$, where $H_{mf} \sim 1$ GeV. However, for the HM interaction the strong momentum-dependent mean field $s(\mathbf{r}, \mathbf{p}, f)$ is created by the density build-up, and the second term in the r.h.s. of (14) becomes large (and positive), which results in a larger transverse velocity for HM. On the other hand, the force acting on a particle depends mostly on the EOS produced by a given mean field or on the pressure gradient. Thus, the r.h.s. of (15) depends relatively weakly on the momentum dependence

of a mean field.

Later on $\langle v_t \rangle$ and $\langle p_t \rangle$ decrease reaching asymptotic values at $t \simeq 50$ fm/c. This decrease is due to less energetic products of NN scattering, which populate the midrapidity region at later times, while first-chance collision products have larger kinetic energies. Faster moving particles (in the case of the HM calculation with respect to H) are shadowed more effectively, which causes a larger splitting between in- and out-of-plane transverse velocities for the HM calculation at large times.

In Fig. 5 we show the final azimuthal angle dependence of the midrapidity neutron transverse velocity (a) and the neutron azimuthal distribution (b). The azimuthal angle modulation of the transverse velocity is clearly visible, which was first observed experimentally [31]. The transverse velocity azimuthal angle dependence and the azimuthal distribution of particles have the same shape. The depletion of the particle yield at $\phi = 0^\circ$ and 180° is caused by a shadowing of fast moving particles by the spectators; the enhanced yield at $\phi = \pm 90^\circ$ correlates with the nonshadowed emission of fast particles.

Fig. 6 shows the coefficient v_2 vs. transverse velocity (left panels) and vs. transverse momentum (right panels) at the two time steps $t = 30$ fm/c and $t = 50$ fm/c. Even at 30 fm/c the particles still feel the influence of the nuclear field and, therefore, the simple relation $v_t = p_t/H_{mf}$ can be applied at this moment only in the case of the momentum-independent mean field H. One can see, that at 30 fm/c the $v_2(p_t)$ -dependence is different for different mean fields, while the $v_2(v_t)$ -dependence is very similar for the H and HM calculations. This is in agreement with our expectation, that particles moving with the same transverse velocity are shadowed in the same way regardless of their transverse momenta. At later times, this "transient universality" of $v_2(v_t)$ is destroyed since the influence of the mean field will become negligible here and $v_t = p_t/\sqrt{m_0^2 + p^2}$ for both parameter sets.

V. COMPARISON WITH EXPERIMENT

In our comparison to data on squeeze-out observables we now compare in parallel also to data on the in-plane flow F , which is defined as the derivative of the transverse in-plane momentum component $\langle p_x \rangle$ with respect to the normalized c.m. rapidity $y^{(0)} = (y/y_{proj})_{c.m.}$ at midrapidity [32]:

$$F = \frac{d\langle p_x \rangle}{dy^{(0)}} \Big|_{y^{(0)}=0} . \quad (16)$$

A simultaneous description of both observables, i.e. v_2 and F , will give a rather strong confidence that the dynamics of the participant zone and the interaction of the participating nucleons with the spectators are described consistently in our calculation and potentially leading to stringent constraints on the EOS and the interactions employed (see also Refs. [33,34] where the energy regime below 100 AMeV has been studied in detail).

Figs. 7-9 show the excitation functions of v_2 and F for protons in case of Au+Au collisions in the impact parameter range $b = 5 \div 7$ fm corresponding to an estimate given in Refs. [28,35]. The data are taken from Refs. [8,35–38]. The time evolution has been followed until $t_{max}=40$ fm/c at $E_{lab}=2$ AGeV, while at smaller beam energies t_{max} gradually increases reaching 250 fm/c at $E_{lab}=25$ AMeV.

The v_2 coefficient (Fig. 7) was calculated for *free* protons in the c.m. rapidity range $|y| < 0.1$. Free protons were selected by the requirement, that the distance to the closest particle within a given parallel ensemble is more than some critical distance $d_c \simeq 3$ fm in order to separate from protons bound in fragments. As discussed in Sect. III, the elliptic flow v_2 vs. E_{lab} shows a nonmonotonic behaviour: it decreases from positive to negative values reaching a minimum at $E_{lab} \simeq 0.4$ AGeV, and then it starts to increase moderately again with beam energy. In this work, however, we only concentrate on the beam energy domain below 2 AGeV and, therefore, the transition from negative to positive v_2 at a beam energy ~ 4 AGeV [28,20] is not discussed here. The lower transition energy, i.e. the beam energy at which v_2 changes sign, is $E_{TRA} \simeq 100$ AMeV, in agreement with the FOPI-data [39]. The

in-plane flow (Figs. 8,9) increases monotonically in the beam energy region considered. The balance energy, i.e. the beam energy at which the flow F changes sign, is $E_{BAL} \simeq 50$ AMeV in our calculation. This value is in between the MSU-data [38] ($E_{BAL} \simeq 42$ AMeV) and the FOPI-data [39] ($E_{BAL} \simeq 60$ AMeV).

Now we discuss the effect of the mean field on v_2 and F . The calculation with a momentum-independent mean field H is in a satisfactory agreement with proton in-plane flow data below 1 AGeV (Fig. 8), but it fails to reproduce the strong squeeze-out at $E_{lab} \simeq 0.4$ AGeV (Fig. 7). The HM parametrization increases the in-plane flow and squeeze-out (see also Fig. 5) and, thus, the in-plane proton flow F is now overpredicted. The lower incompressibility K in the SM calculation results in a reduced squeeze-out and a reduced flow with respect to the HM calculation. Generally, the in-plane proton flow and v_2 data are best reproduced with the SM mean field.

In Fig. 9 we compare to FOPI, EOS and recent MSU-4 π data on the in-plane flow excitation function. The selected data sets are now for a mixture of protons and complex fragments and, therefore, they exhibit a stronger flow signal (c.f. Fig. 8, where the data are for protons only). A separate study of the fragment flow is out of scope of this work. However, in order to understand qualitatively the possible effects from cluster formation, we present in Fig. 9 the results of the BUU-SM calculation both for *all* (solid line) and *free* (dashed line) protons. We find a steeper increase of the in-plane flow for *all* protons with the beam energy from 0.1 to 1 AGeV. The calculation for *all* protons is in a good agreement with data at $E_{lab} = 0.4 \div 1$ AGeV, but it underpredicts the flow at lower beam energies, where the *free* proton flow F increases earlier with E_{lab} and is closer to the data. This can be explained by the cluster formation scenario from initially *free* emitted protons by the momentum (rather than coordinate) space coalescence. The balance energy given by the SM calculation is $E_{bal} \simeq 50$ (60) AMeV for *free* (*all*) protons, which is somewhat larger than the value $E_{bal} \simeq 42$ AMeV reported in [38]. But the shape of the in-plane flow excitation function at $E_{lab} = 25 \div 60$ AMeV is in a remarkable agreement with the MSU-4 π data. We would like to stress, that the negative in-plane flow in the Au+Au system below E_{BAL} is

obtained in our calculations taking into account initial repulsive Rutherford-trajectories (c.f. Ref. [34], where an opposite result has been obtained).

In Fig. 10 we present the midrapidity neutron azimuthal distributions with respect to the in-plane flow axis for the reactions Nb+Nb and La+La at 400 AMeV in comparison to the data from Ref. [40] (see Fig. 11 of [40]). In this comparison the BUU events were treated as the experimental data [40], i.e. the azimuthal angle of the reaction plane was defined by the \mathbf{Q} vector:

$$\mathbf{Q} = \sum_{\nu} w^{\nu} \frac{\mathbf{v}_t^{\nu}}{|\mathbf{v}_t^{\nu}|}, \quad (17)$$

where the sum is taken over all charged fragments (i.e. all protons in BUU); \mathbf{v}_t^{ν} is the transverse velocity of the particle ν ; $w^{\nu} = 1$ for $y^{(0)} \geq 0.2$, $w^{\nu} = 0$ for $-0.2 \leq y^{(0)} \leq 0.2$, $w^{\nu} = -1$ for $y^{(0)} < -0.2$. Furthermore, we have determined the flow angle Θ_F by diagonalizing the flow tensor F_{ij} in the c.m.s. (see [41]):

$$F_{ij} = \sum_{\nu} \frac{1}{2m_0} \frac{v_i^{\nu} v_j^{\nu}}{|\mathbf{v}^{\nu}|^2}. \quad (18)$$

Finally, a rotation of the c.m. coordinate system was performed, first, around the beam z-axis to align the x-axis with the vector \mathbf{Q} and, second, around the y-axis by the flow angle Θ_F (see Refs. [42,43]). As shown in Refs. [42,43], the squeeze-out is more pronounced in the rotated coordinate system (x', y', z') . The azimuthal distributions in Fig. 10 are presented for neutrons with longitudinal momenta $-0.1 \leq (p'_z/p'_{proj})_{c.m.} \leq 0.1$. We see from Fig. 10, that the data can be reasonably well reproduced adopting the HM1 mean field (see Table 1), suggesting that the MDI stiffness C in the parameter set HM is not high enough. Our conclusion is in line with the results of Ref. [40], where it was reported that BUU calculations with the mean field of [24] ($K = 215$ MeV, i.e. the SM parametrization) underpredict the squeeze-out.

Fig. 11 shows the in-plane transverse momentum $\langle p_x \rangle$ of neutrons versus the normalized rapidity $y^{(0)}$ for the reactions Nb+Nb and La+La at 400 AMeV. We observe that an increased MDI stiffness improves the agreement with the neutron in-plane flow data, too.

Finally, we have studied the neutron squeeze-out in Au+Au collisions measured by the FOPI-LAND Collaboration [44]. Fig. 12 shows the impact parameter dependence of the squeeze-out ratio R_N for Au+Au collisions at 400 AMeV, which reasonably describes the data for the HM calculation (dotted histogram). The HM1 parameter set (solid histogram) underpredicts somewhat the squeeze-out ratio in central collisions and overpredicts it in semiperipheral ($b = 7 \div 8$ fm) collisions. The SM parameter set (dash-dotted histogram) and momentum-independent field H (dashed histogram) underpredict the data at large impact parameters. The calculated $R_N(b)$ -dependence has a characteristic bell-shape with a maximum at $b \simeq 7$ fm. This agrees with the results of Ref. [39], where the squeeze-out was studied for charged particles. The drop of R_N at large impact parameters can be explained by a smaller compression of the participant zone and, therefore, smaller transverse velocities of particles emitted in peripheral collisions.

In Fig. 13 the p_t -dependence of the ratio R_N is shown for collisions of Au+Au at 400, 600 and 800 AMeV. In agreement with the previous calculations of Ref. [18] we observe that a lower effective mass, i.e. a steeper momentum dependence, increases the squeeze-out ratio R_N at large p_t (c.f. dotted and solid lines in Fig. 13 d-f). On the other hand, reducing the NN cross section decreases the ratio R_N at large p_t (c.f. solid and long-dashed lines in Fig. 13 e). The parameter set H produces a too flat $R_N(p_t)$ -dependence (c.f. short-dashed line in Fig. 13 a). The SM calculation gives the best overall agreement with the data (dash-dotted line in Fig. 13 a-c). We see that our BUU calculations reproduce the experimentally observed trend of R_N to decrease (at fixed p_t) with collision energy, which was interpreted in Ref. [44] as a scaling behaviour of the squeeze-out.

VI. SUMMARY AND CONCLUSIONS

The squeeze-out of nuclear matter in heavy-ion collisions at beam energies $E_{lab} = 0.05 \div 2$ AGeV has been studied within the BUU approach of Ref. [21]. As demonstrated, being essentially caused by the shadowing of the expanding fireball by cold spectators, the squeeze-

out is quite sensitive to the specific velocity of the particles. A mean field with a larger MDI stiffness gives a smaller effective mass, and thus a harder velocity spectrum of nucleons. In a heavy-ion collision thus faster moving nucleons are shadowed more effectively and the squeeze-out ratio R_N is larger for mean fields with stronger momentum dependence.

The systematic comparison with the experimental data on the excitation function of the elliptic flow v_2 [8] favours mean fields with $m^* \simeq 0.68m_0$, i.e. HM or SM sets. The influence of the incompressibility K on the squeeze-out turns out to be quite weak. The proton in-plane flow data of the EOS Collaboration at $E_{lab} = 0.25 \div 1.15$ AGeV and the fragment flow data of the MSU-4 π Collaboration at $E_{lab} = 25 \div 60$ AMeV are consistent with the SM mean field. We have found, that a reproduction of the BERKELEY data [40] on the neutron azimuthal distributions and the in-plane flow in Nb+Nb and La+La collisions at 400 AMeV requires an enhanced MDI stiffness for $p < 1$ GeV/c (HM1 parameter set: $K = 379$ MeV and $m^* = 0.62m_0$). However, the FOPI-LAND data [44] on the neutron squeeze-out in Au+Au collisions at 400 \div 800 AMeV favour the standard MDI stiffness (HM or SM parameter sets).

To conclude, a simultaneous description of the nucleon squeeze-out v_2 and the in-plane flow F at the beam energies $E_{lab} = 0.2 \div 2$ AGeV requires a mean field with a strong momentum dependence. This corresponds to an effective Landau mass at the Fermi surface $m^*/m_0 = 0.65 \pm 0.03$ at normal nuclear density. The incompressibility K , however, is less well determined since in semiperipheral reactions the average density probed up to 1 AGeV is too low.

ACKNOWLEDGMENTS

One of us (A.B.L.) is grateful to P. Danielewicz, W. G. Lynch, M. B. Tsang and G. D. Westfall for useful discussions during his stay at MSU, and to P. Danielewicz for pointing out the importance of a proper fragment selection in the comparison with fragment flow data.

REFERENCES

- [1] W. Scheid, R. Ligensa, and W. Greiner, Phys. Rev. Lett. **21**, 1479 (1968).
- [2] H. Stöcker and W. Greiner, Phys. Rep. **137**, 277 (1986).
- [3] G.F. Bertsch and S. Das Gupta, Phys. Rep. **160**, 189 (1988).
- [4] H.H. Gutbrod, A.M. Poskanzer, and H.G. Ritter, Rep. Prog. Phys. **52**, 1267 (1989).
- [5] J. Aichelin, Phys. Rep. **202**, 233 (1991).
- [6] W. Reisdorf and H.G. Ritter, Annu. Rev. Nucl. Part. Sci. **47**, 1 (1997).
- [7] P.K. Sahu, A. Hombach, W. Cassing, M. Effenberger, U. Mosel, Nucl. Phys. **A640**, 493 (1998).
- [8] N. Herrmann, J.P. Wessels, and T. Wienold, Annu. Rev. Nucl. Part. Sci. **49**, 581 (1999).
- [9] A. Hombach, W. Cassing, S. Teis and U. Mosel, Eur. Phys. J. A **5**, 157 (1999).
- [10] C. Gale, G. Bertsch, S. Das Gupta, Phys. Rev. C **35**, 1666 (1987).
- [11] J. Aichelin, A. Rosenhauer, G. Peilert, H. Stöcker, and W. Greiner, Phys. Rev. Lett. **58**, 1926 (1987).
- [12] C. Gale, G.M. Welke, M. Prakash, S.J. Lee, and S. Das Gupta, Phys. Rev. C **41**, 1545 (1990).
- [13] J. Zhang, S. Das Gupta, and C. Gale, Phys. Rev. C **50**, 1617 (1994).
- [14] P. Danielewicz and G. Odyniec, Phys. Lett. **157B**, 146 (1985).
- [15] H.M. Xu, Phys. Rev. Lett. **67**, 2769 (1992); Phys. Rev. C **46**, R392 (1992).
- [16] V.N. Russkikh, Yu.B. Ivanov, Yu.E. Pokrovsky, P.A. Henning, Nucl. Phys. **A572**, 749 (1994).
- [17] A. Hombach, W. Cassing, and U. Mosel, Eur. Phys. J. A **5**, 77 (1999).

- [18] P. Danielewicz, Nucl. Phys. **A673**, 375 (2000).
- [19] D. Brill, P. Beckerle, C. Bormann, E. Schwab, Y. Shin, R. Stock, H. Ströbele, P. Baltes, C. Müntz, H. Oeschler, C. Sturm, A. Wagner, R. Barth, M. Cieřlak, M. Dębowski, E. Grosse, P. Koczoń, M. Mang, D. Miřkowiec, R. Schicker, P. Senger, B. Kohlmeyer, F. Pühlhofer, J. Speer, K. Völkel, W. Waluś, Z. Phys. A **355**, 61 (1996).
- [20] P.K. Sahu, W. Cassing, U. Mosel and A. Ohnishi, Nucl. Phys. **A672**, 376 (2000).
- [21] M. Effenberger, E.L. Bratkovskaya, and U. Mosel, Phys. Rev. C **60**, 044614 (1999).
- [22] J. Cugnon, D. L'Hôte, J. Vandermeulen, Nucl. Instrum. Methods Phys. Res. B **111**, 215 (1996).
- [23] S. Teis, W. Cassing, M. Effenberger, A. Hombach, U. Mosel, and G. Wolf, Z. Phys. A **356**, 421 (1997).
- [24] G.M. Welke, M. Prakash, T.T.S. Kuo, S. Das Gupta, and C. Gale, Phys. Rev. C **38**, 2101 (1988).
- [25] Madappa Prakash, Ignazio Bombaci, Manju Prakash, Paul J. Ellis, James M. Lattimer, Roland Knorren, Phys. Rep. **280**, 1 (1997).
- [26] E. Chabanat, P. Bonche, P. Haensel, J. Meyer, R. Schaeffer, Nucl. Phys. **A627**, 710 (1997).
- [27] H. Appelshäuser et al. (NA49 Collaboration), Phys. Rev. Lett. **80**, 4136 (1998).
- [28] C. Pinkenburg et al. (E895 Collaboration), Phys. Rev. Lett. **83**, 1295 (1999).
- [29] J. Gosset, H.H. Gutbrod, W.G. Meyer, A.M. Poskanzer, A. Sandoval, R. Stock, and G.D. Westfall, Phys. Rev. C **16**, 629 (1977).
- [30] M.B. Tsang, P. Danielewicz, W.C. Hsi, M. Huang, W.G. Lynch, D.R. Bowman, C.K. Gelbke, M.A. Lisa, G.F. Peaslee, R.J. Charity, L.G. Sobotka, and ALADIN Collabora-

- tion, Phys. Rev. C **53**, 1959 (1996).
- [31] G. Rai et al., Nucl. Phys. **A661**, 162c (1999).
- [32] K.G.R. Doss, H.Å. Gustafsson, H.H. Gutbrod, K.H. Kampert, B. Kolb, H. Löhner, B. Ludewigt, A.M. Poskanzer, H.G. Ritter, H.R. Schmidt, and H. Wieman, Phys. Rev. Lett. **57**, 302 (1986).
- [33] Yu-Ming Zheng, C.M. Ko, Bao-An Li, and Bin Zhang, Phys. Rev. Lett. **83**, 2534 (1999).
- [34] S. Soff, S.A. Bass, C. Hartnack, H. Stöcker and W. Greiner, Phys. Rev. C **51**, 3320 (1995).
- [35] M.D. Partlan et al. (EOS Collaboration), Phys. Rev. Lett. **75**, 2100 (1995).
- [36] H. Liu et al. (E895 Collaboration), Nucl. Phys. **A638**, 451c (1998).
- [37] H. Liu et al. (E895 Collaboration), Phys. Rev. Lett. **84**, 5488 (2000).
- [38] D.J. Magestro, W. Bauer, O. Bjarki, J.D. Crispin, M.L. Miller, M.B. Tonjes, A.M. Vander Molen, G.D. Westfall, R. Pak, E. Norbeck, Phys. Rev. C **61**, 021602(R) (2000).
- [39] P. Crochet et al. (FOPI Collaboration), Nucl. Phys. **A624**, 755 (1997).
- [40] M.M. Htun, R. Madey, W.M. Zhang, M. Elaasar, D. Keane, B.D. Anderson, A.R. Baldwin, J. Jiang, A. Scott, Y. Shao, J.W. Watson, K. Frankel, L. Heilbronn, G. Krebs, M.A. McMahan, W. Rathbun, J. Schambach, G.D. Westfall, S. Yennello, C. Gale, and J. Zhang, Phys. Rev. C **59**, 336 (1999).
- [41] M. Gyulassy, K.A. Frankel and H. Stöcker, Phys. Lett. **110B**, 185 (1982).
- [42] H.H. Gutbrod, K.H. Kampert, B.W. Kolb, A.M. Poskanzer, H.G. Ritter and H.R. Schmidt, Phys. Lett. **216B**, 267 (1989).
- [43] H.H. Gutbrod, K.H. Kampert, B. Kolb, A.M. Poskanzer, H.G. Ritter, R. Schicker, and H.R. Schmidt, Phys. Rev. C **42**, 640 (1990).

- [44] D. Lambrecht, T. Blaich, T.W. Elze, H. Emling, H. Freiesleben, K. Grimm, W. Henning, R. Holzmann, J.G. Keller, H. Klingler, J.V. Kratz, R. Kulesa, S. Lange, Y. Leifels, E. Lubkiewicz, E.F. Moore, W. Prokopowicz, R. Schmidt, C. Schütter, H. Spies, K. Stelzer, J. Stroth, E. Wajda, W. Waluś, M. Zinser, E. Zude, and FOPI Collaboration, *Z. Phys. A* **350**, 115 (1994).

Table 1. Parameter sets for the different mean fields employed in the BUU calculation.

Not.	K (MeV)	m^*/m_0	A (MeV)	B (MeV)	C (MeV)	τ	Λ (fm $^{-1}$)
H	380	1.00	-124.3	71.0	0.0	2.00	-
HM	379	0.68	-10.0	38.0	-63.6	2.40	2.13
HM1	379	0.62	22.2	29.5	-82.7	2.62	2.13
SM	220	0.68	-108.6	136.8	-63.6	1.26	2.13

FIGURE CAPTIONS

Fig. 1 Density dependence of the energy per nucleon in nuclear matter (upper left panel). The other three panels show the mean-field potential vs. momentum at the nuclear densities $0.5\rho_0$, ρ_0 and $2\rho_0$. The dashed, dotted, solid and dash-dotted lines correspond to the interactions H, HM, HM1 and SM, respectively.

Fig. 2 Central baryon density (smooth lines, left scale) and NN collision rate (histograms, right scale) vs. time for Au+Au at 0.4 AGeV and $b = 6$ fm. The solid (dashed) line and histogram correspond the HM (SM) calculation. The horizontal dotted line shows the normal nuclear density ρ_0 for comparison.

Fig. 3 Average transverse velocity (a) and transverse momentum (b) of neutrons in the c.m. rapidity range $|y| < 0.1$ emitted in the reaction plane ($\phi = -30^\circ \div 30^\circ$, $150^\circ \div 180^\circ$, $-180^\circ \div -150^\circ$) and out of the reaction plane ($\phi = 60^\circ \div 120^\circ$, $-60^\circ \div -120^\circ$) for Au+Au at 400 AMeV and $b = 6$ fm.

Fig. 4 Time evolution of the baryon density in the reaction plane (x, z) for Au+Au at 0.4 AGeV and $b = 6$ fm calculated with the HM mean field. Isolines from outer to inner correspond to densities in the order 0.05, 0.1, 0.15, 0.20 and 0.25 fm^{-3} .

Fig. 5 (a) Azimuthal dependence of the average neutron velocity and (b) neutron azimuthal distribution for Au+Au at 0.4 AGeV and $b = 5 \div 7$ fm. Neutrons are selected in the c.m. rapidity interval $|y| < 0.1$. The corresponding elliptic flows are: $v_2 = -0.046$ (H) and $v_2 = -0.090$ (HM).

Fig. 6 The elliptic flow v_2 vs. transverse velocity (left panels) and vs. transverse momentum (right panels) of neutrons in the c.m. rapidity interval $|y| < 0.1$ for the time steps $t = 30 \text{ fm}/c$ (upper panels) and $t = 50 \text{ fm}/c$ (lower panels). The calculations have been performed with the H (open circles, dashed line) and HM (full circles, solid line) parameter sets. The system is Au+Au at 0.4 AGeV and $b = 6$ fm.

Fig. 7 Excitation function of the elliptic flow v_2 as given by the collection of experimental data from various groups [8] and by the BUU calculations. The BUU curves are shown for Au+Au collisions at $b = 5 \div 7$ fm for *free* (unbound) protons with a critical distance $d_c = 3$ fm in the c.m. rapidity range $|y| < 0.1$ (see text). The curves correspond to various mean-field parameter sets: short-dashed – H, thick solid – SM, dotted – HM. For reference the results of the cascade calculation (without mean field) are shown by the thin solid line.

Fig. 8 Excitation function of the transverse in-plane flow F for Au+Au collisions in comparison to the EOS [35] and E895 [37] proton data. The BUU curves are marked as in Fig. 7. The BUU results are impact parameter weighted in the interval $b = 5 \div 7$ fm and are obtained for *free* (unbound) protons with a critical distance $d_c = 3$ fm in the normalized c.m. rapidity range $-0.2 < y^{(0)} < 0.3$.

Fig. 9 Excitation function of the transverse in-plane flow F for Au+Au collisions calculated with the SM mean field for *free* protons ($d_c = 3$ fm, dashed line) and *all* protons ($d_c = 0$ fm, solid line) in comparison to the experimental data of the MSU-4 π Collaboration for $Z = 2$ fragments [38] and with the data of the EOS and FOPI Collaborations for $Z = 1 \div 2$ fragments [36]. The BUU results are weighted in the impact parameter interval $b = 5 \div 7$ fm.

Fig. 10 Azimuthal distributions of neutrons with respect to the flow axis (ϕ') for collisions of Nb+Nb and La+La at 0.4 AGeV in comparison to the data (histograms) from Ref. [40]. Solid and dashed lines correspond to BUU calculations with HM1 and HM mean-field parametrizations, respectively. The BUU results are weighted in the impact parameter range $b = 1 \div 5$ fm (Nb+Nb) and $b = 1 \div 6$ fm (La+La) according to the estimate $b_{max} = 0.5(R_p + R_t)$ in [40]. In the calculations we selected *free* neutrons ($d_c = 3$ fm) with longitudinal momenta $-0.1 \leq (p'_z/p'_{proj})_{c.m.} \leq 0.1$.

Fig. 11 Average neutron transverse in-plane momentum vs. normalized c.m. rapidity for

Nb+Nb and La+La collisions at 0.4 AGeV in comparison to the data from [40]. The BUU results are weighted in the impact parameter range $b = 1 \div 5$ fm (Nb+Nb) and $b = 1 \div 6$ fm (La+La); free neutrons with a critical distance $d_c = 3$ fm are selected in the BUU calculations. The solid and dashed lines correspond to the HM1 and HM parametrizations. The experimental threshold laboratory kin. energy of 55 MeV for neutrons [40] is taken into account which leads to the asymmetric $\langle p_x \rangle(y^{(0)})$ -dependence with respect to $y^{(0)} = 0$.

Fig. 12 The neutron squeeze-out ratio R_N vs. impact parameter b for Au+Au collisions at 400 AMeV. The data from Ref. [44] are for neutrons in the rapidity interval $0.4 \leq y/y_{proj} < 0.6$, while the histograms represent the BUU calculations with various mean-field parameter sets. Upper panel: short-dashed – H, dash-dotted – SM. Lower panel: dotted – HM, solid – HM1. In the BUU calculations free neutrons are selected with $d_c = 3$ fm and the angular cuts of the LAND detector are taken into account. The calculated azimuthal distributions are shown with respect to the reaction plane given by the \mathbf{Q} vector (see text).

Fig. 13 Squeeze-out ratio of neutrons R_N in the rapidity interval $0.4 \leq y/y_{proj} < 0.6$ as a function of the neutron transverse momentum for collisions of Au+Au at 400, 600 and 800 AMeV. The data are from Ref. [44]; the histograms show the BUU calculations for different mean fields: short-dashed – H, dotted – HM, solid – HM1, dash-dotted – SM, long-dashed – HM1 with reduced (by 30%) NN cross section. The BUU results are impact parameter weighted in the region $b = 5 \div 9$ fm, which approximately corresponds to the centrality bin E2 for the data. In the calculations the reaction plane was determined by the \mathbf{Q} vector.

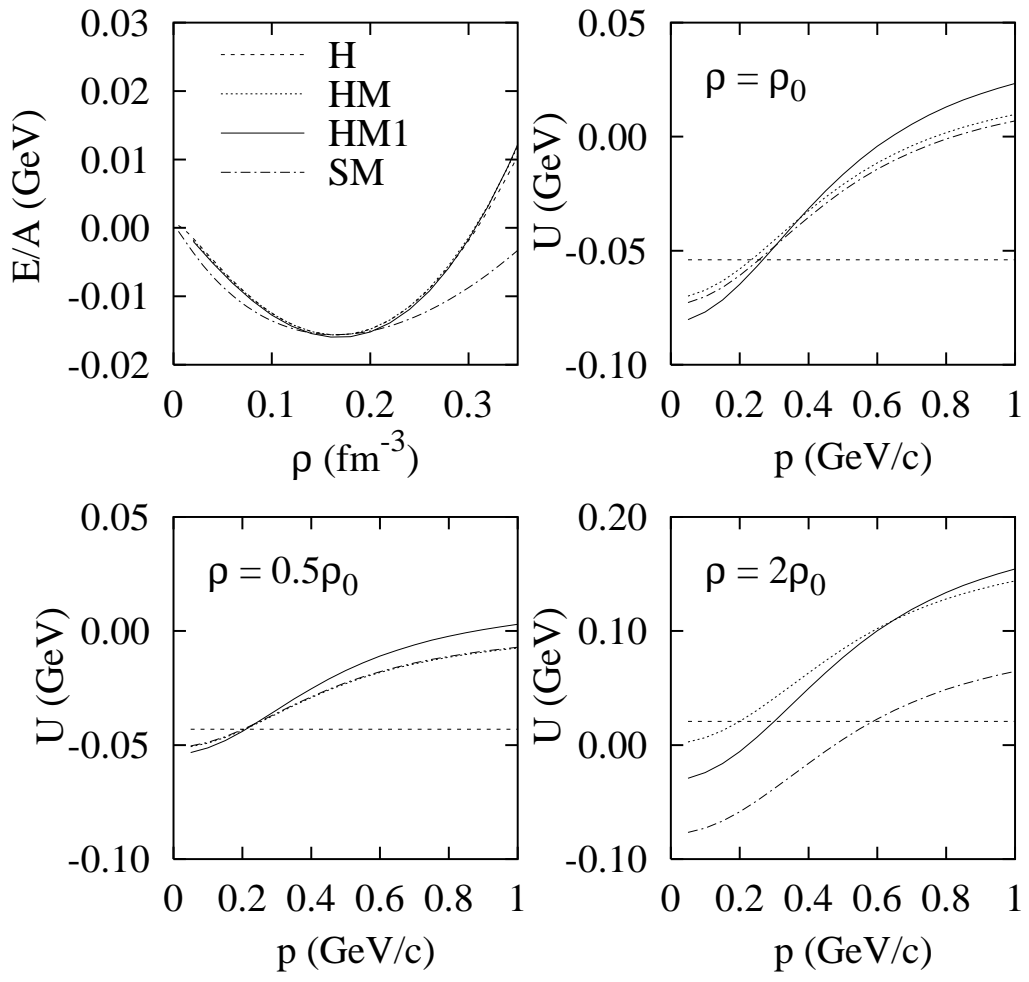


FIG. 1.

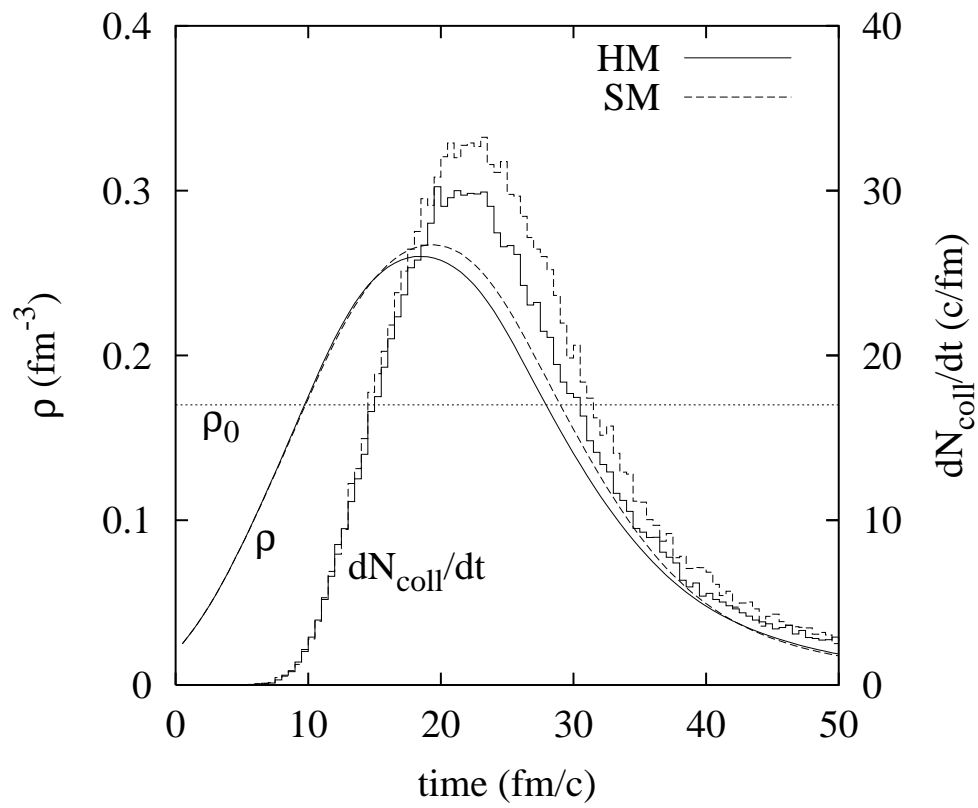


FIG. 2.

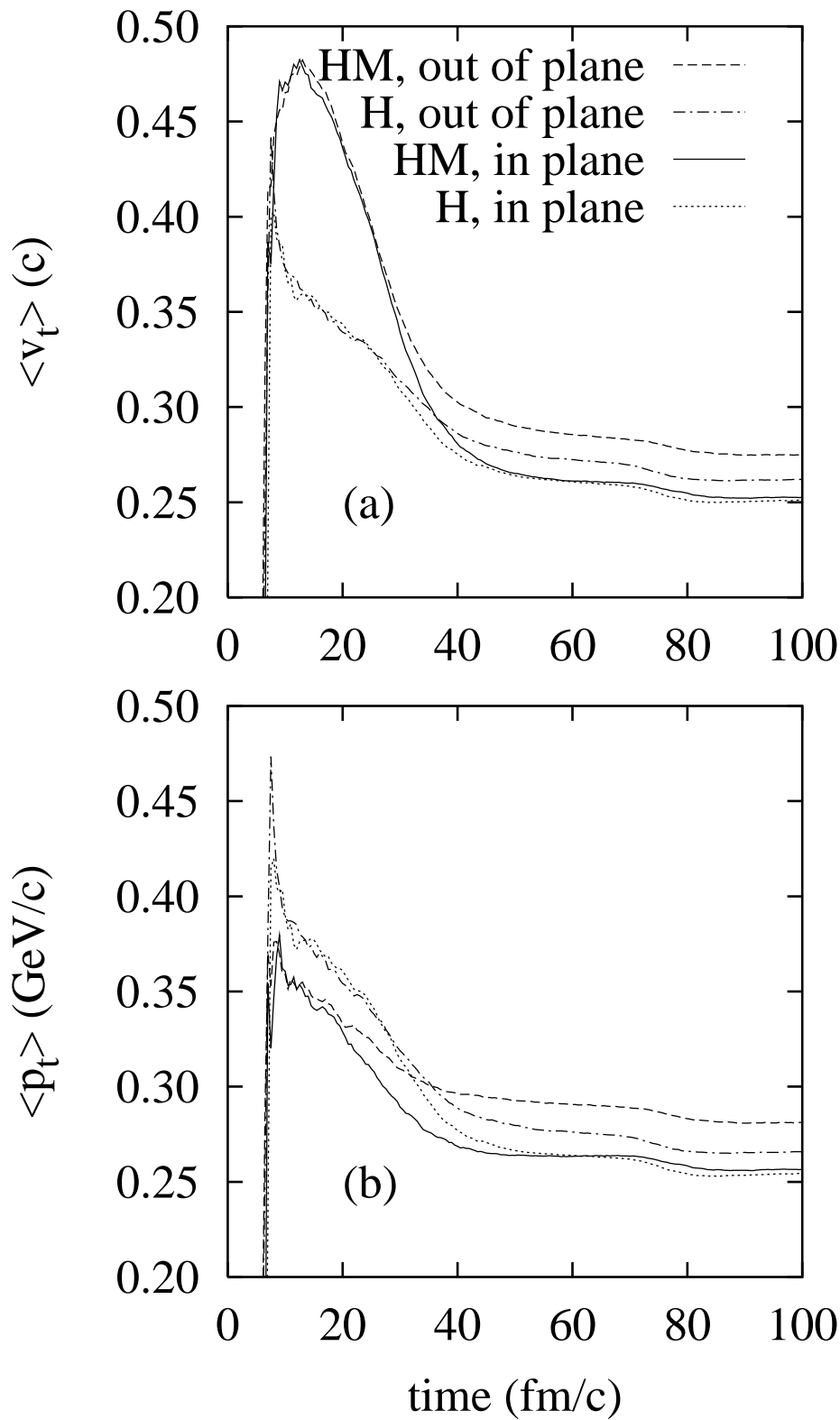


FIG. 3.

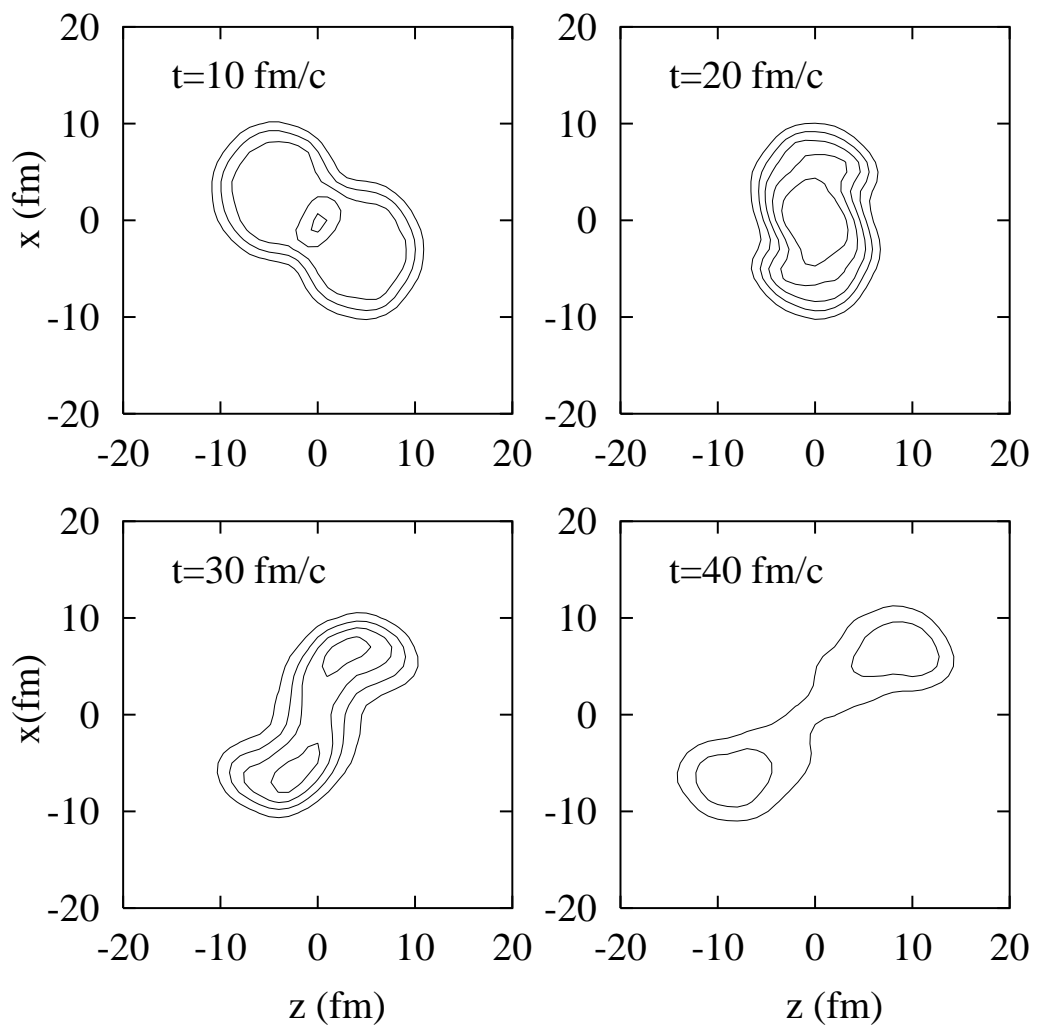


FIG. 4.

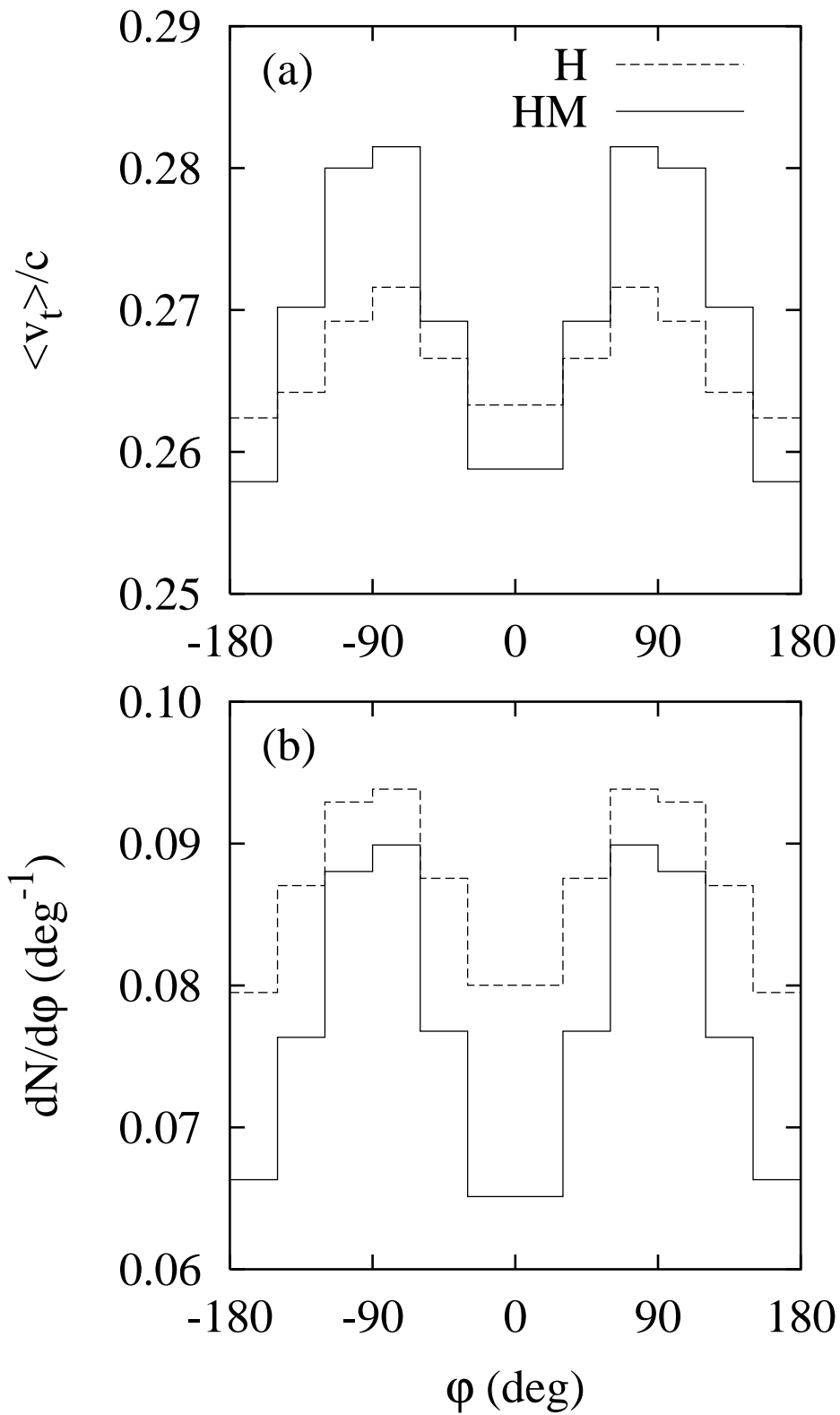


FIG. 5.

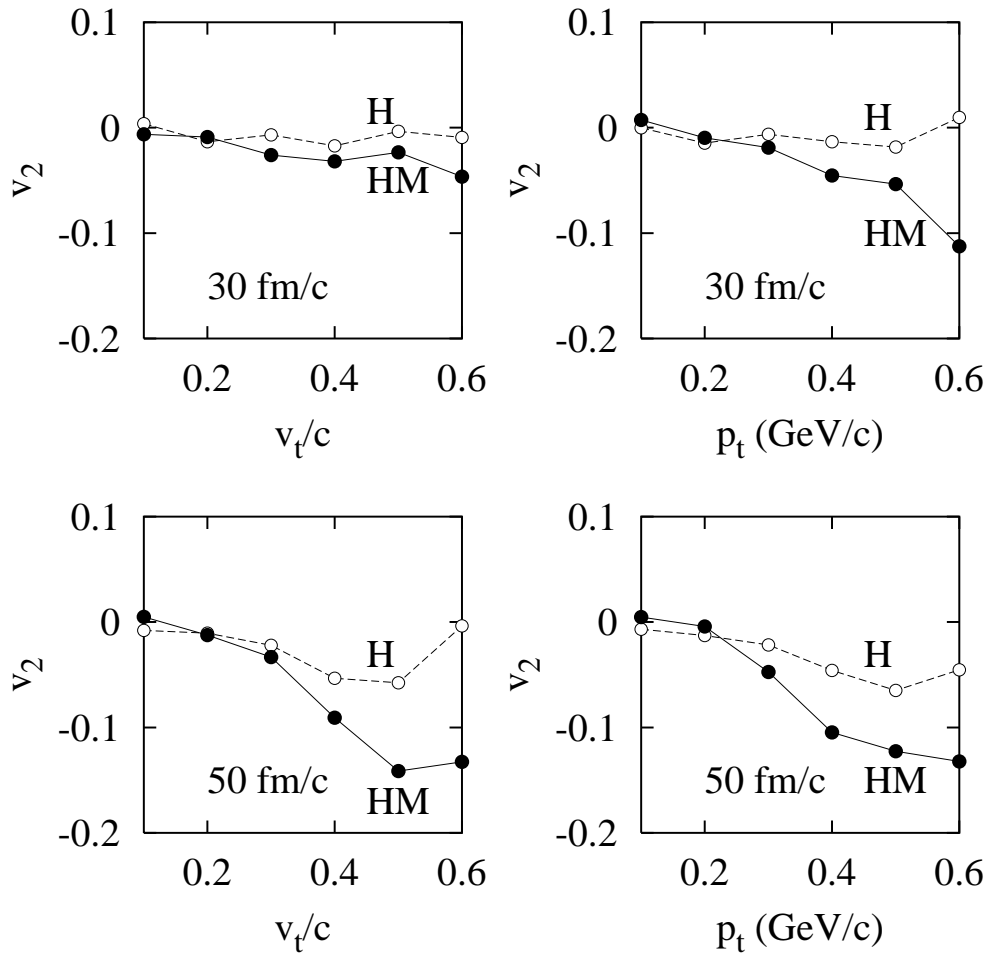


FIG. 6.

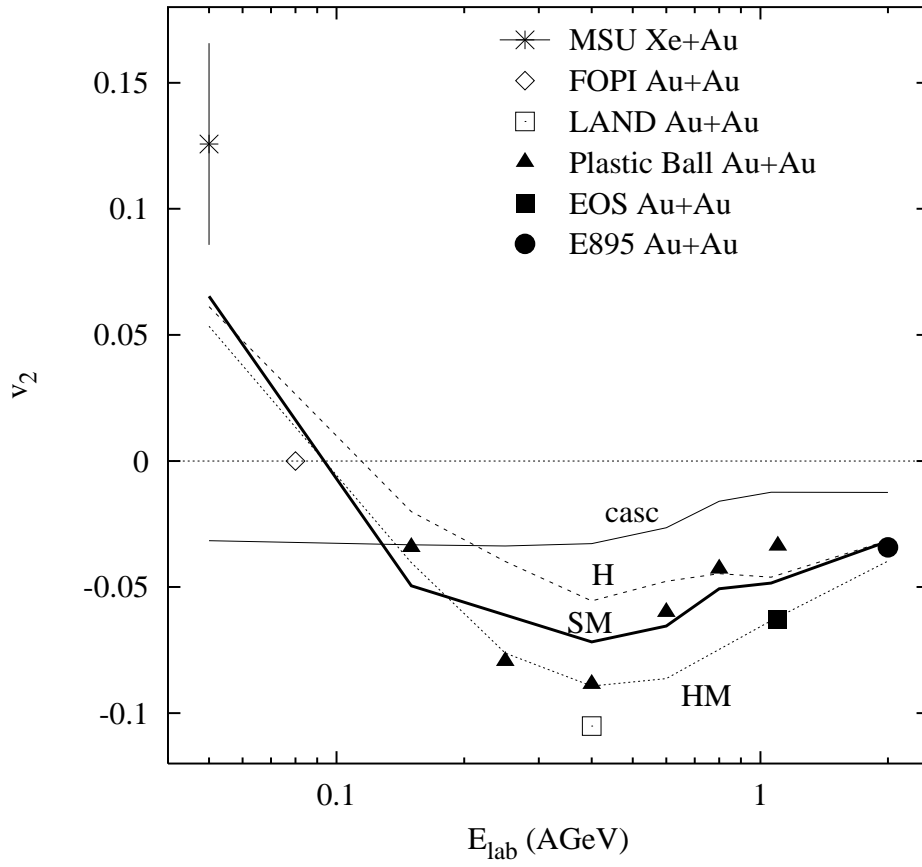


FIG. 7.

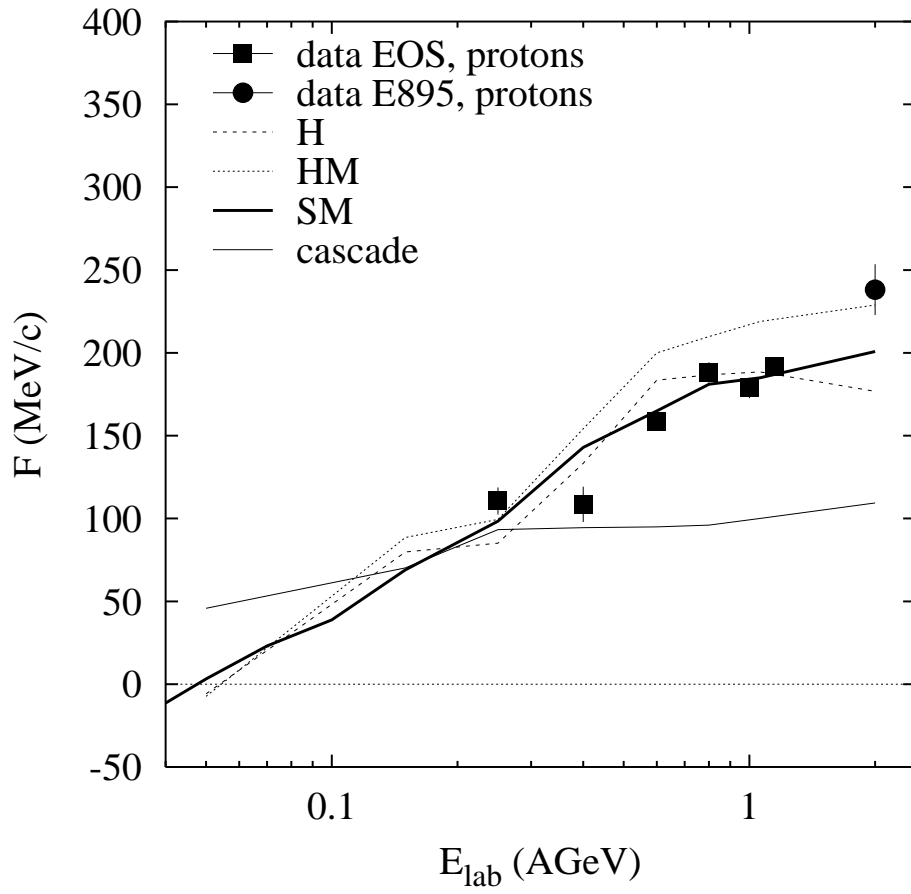


FIG. 8.

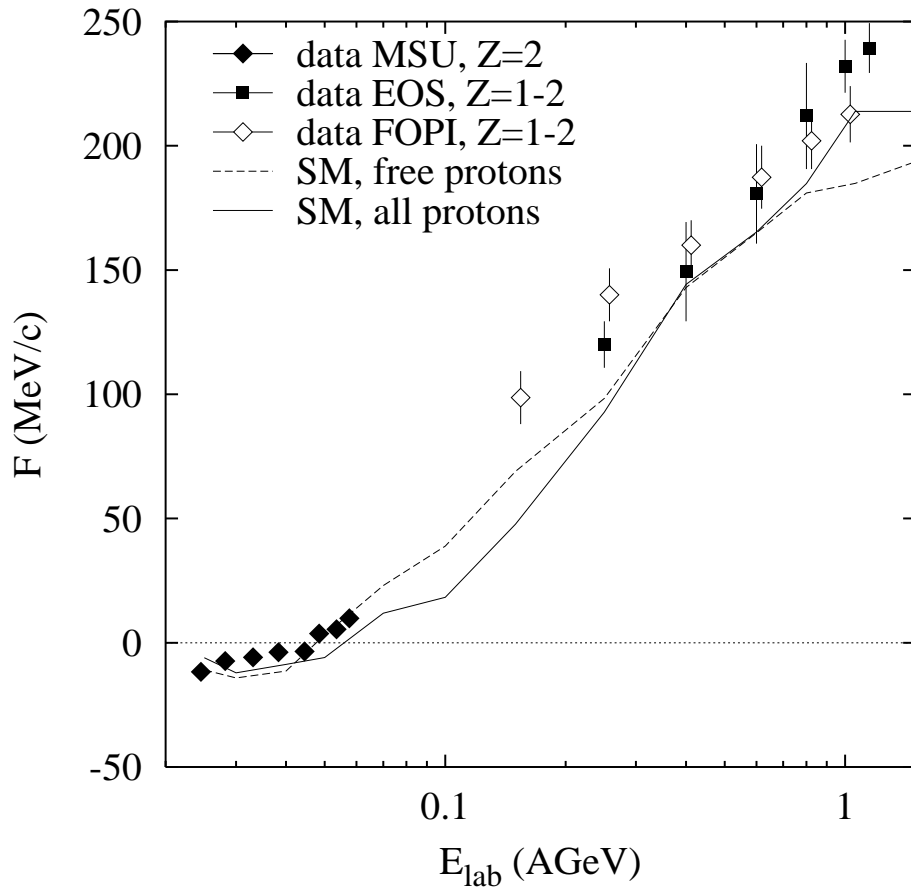


FIG. 9.

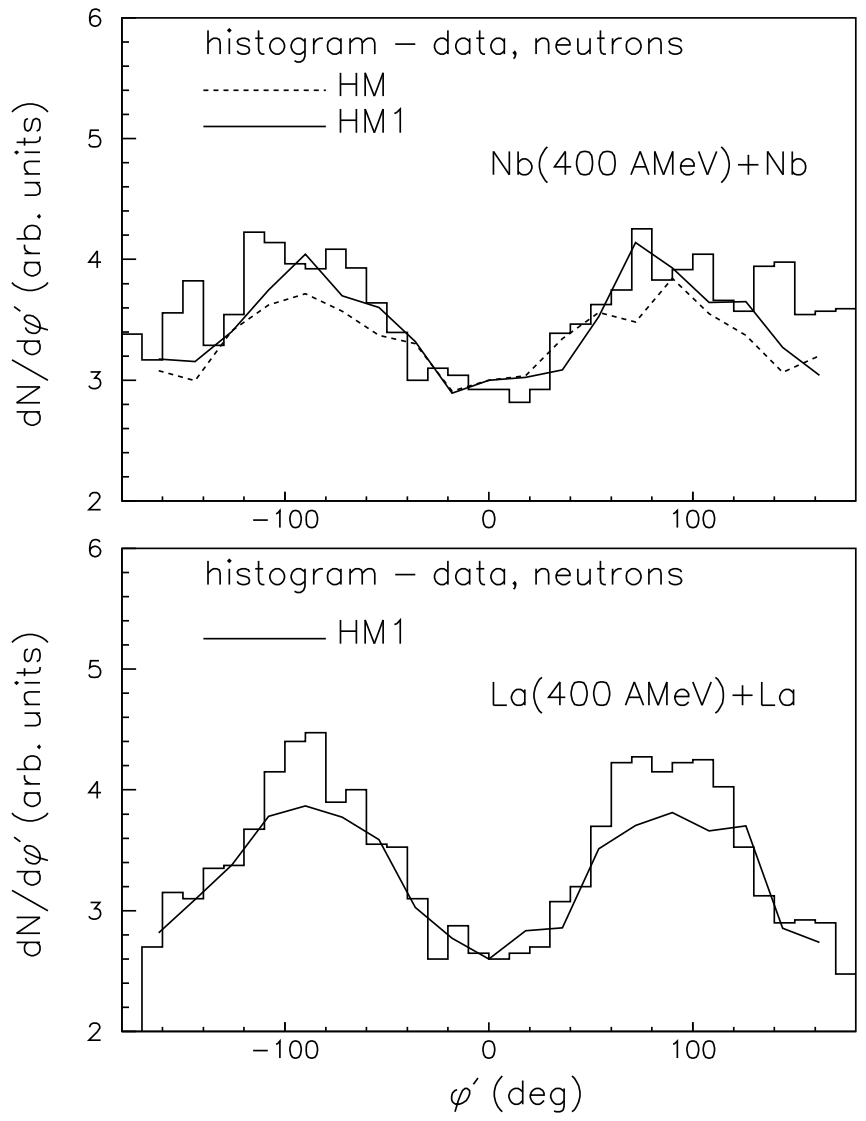


FIG. 10.

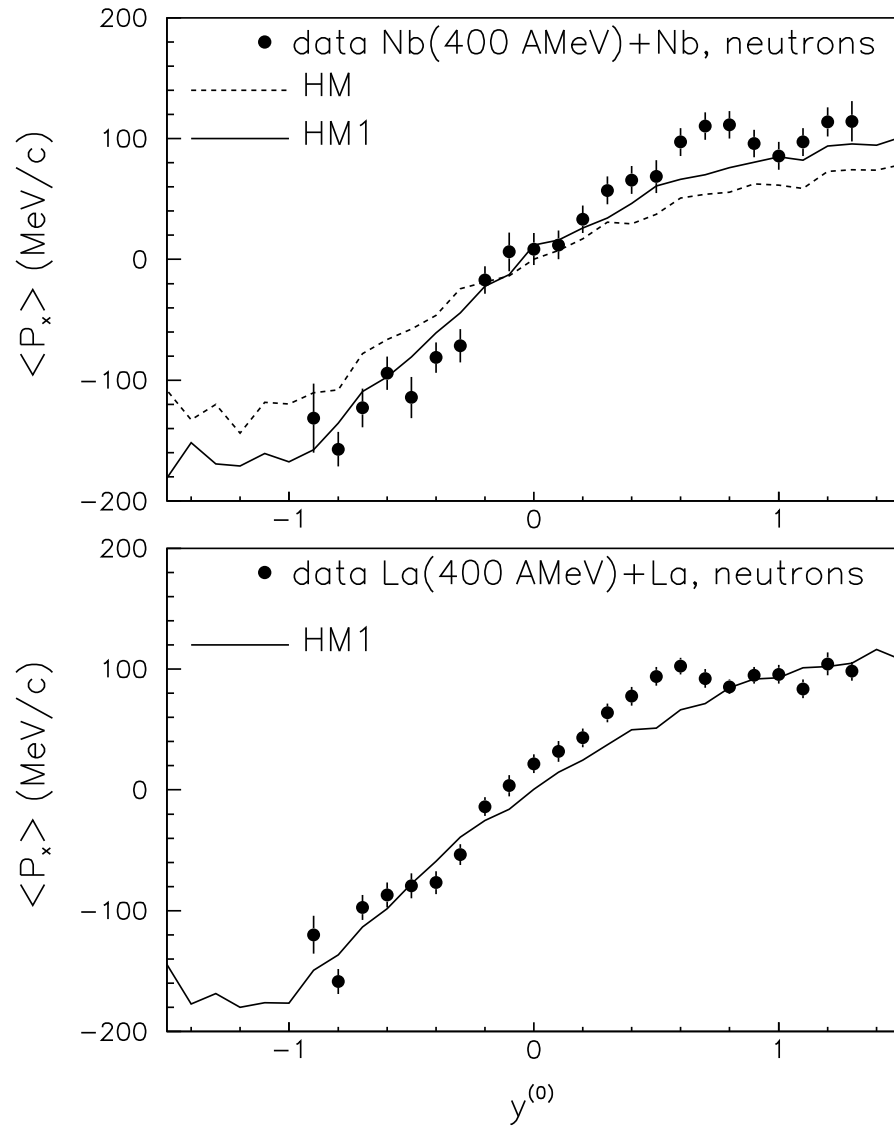


FIG. 11.

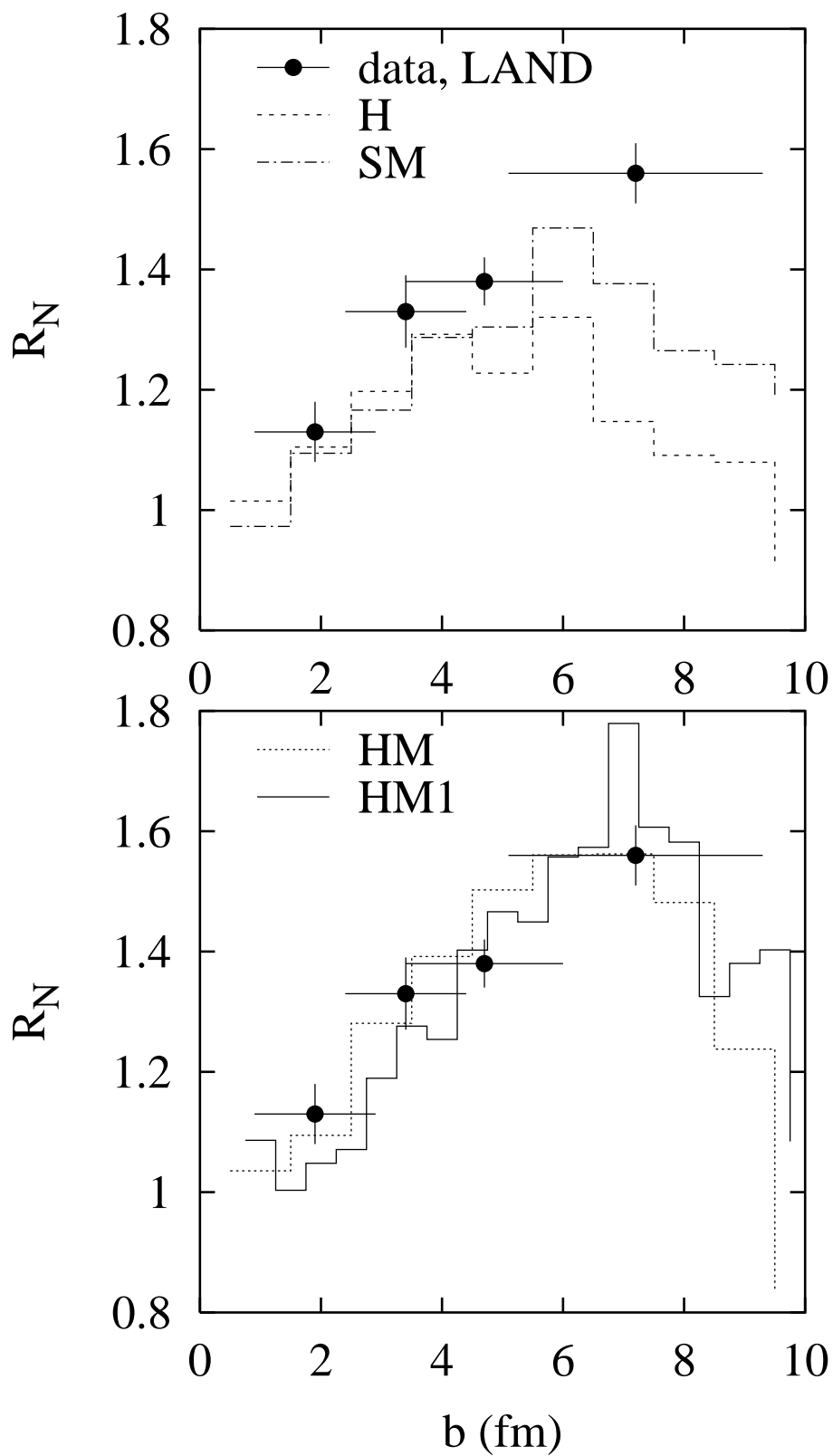


FIG. 12.

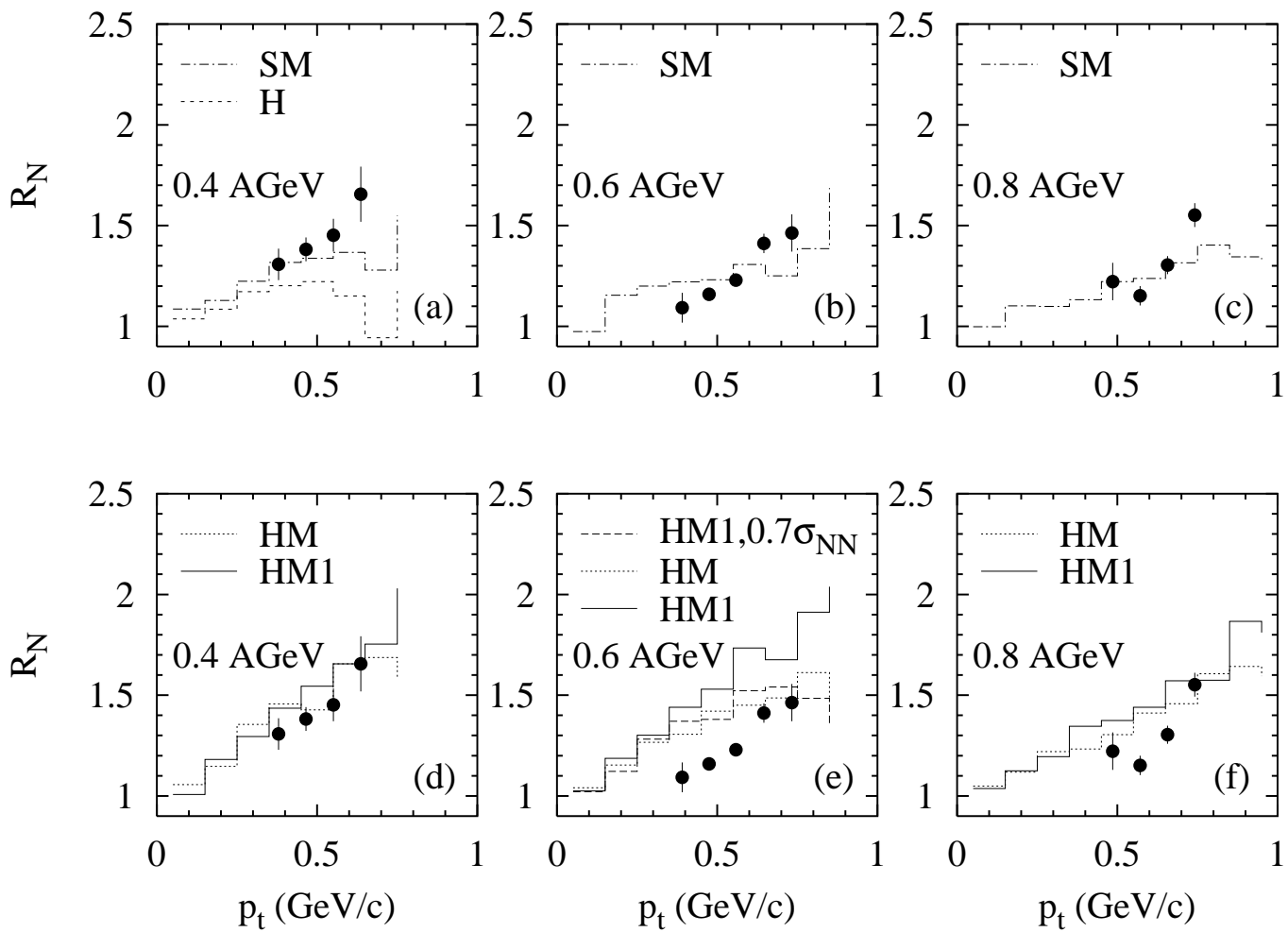


FIG. 13.